Original Article

# Uncertainty analysis of heat transfer of TMSR-SF0 simulator

Jiajun Wang [a,b,c], Ye Dai [a,c], Yang Zou [a,c,*], Hongjie Xu [a,b,c]

[a] *Shanghai Institute of Applied Physics, Chinese Academy of Sciences, Shanghai 201800, China*
[b] *School of Physical Science and Technology, ShanghaiTech University, Shanghai 201210, China*
[c] *University of Chinese Academy of Sciences, Beijing 101408, China*

## A B S T R A C T

The TMSR-SF0 simulator is an integral effect thermal-hydraulic experimental system for the development of thorium molten salt reactor (TMSR) program in China. The simulator has two heat transport loops with liquid FLiNaK. In literature, the 95% level confidence uncertainties of the thermophysical properties of FLiNaK are recommended, and the uncertainties of density, heat capacity, thermal conductivity and viscosity are $\pm 2\%$, $\pm 10$, $\pm 10\%$ and $\pm 10\%$ respectively. In order to investigate the effects of thermophysical properties uncertainties on the molten salt heat transport system, the uncertainty and sensitivity analysis of the heat transfer characteristics of the simulator system are carried out on a RELAP5 model. The uncertainties of thermophysical properties are incorporated in simulation model and the Monte Carlo sampling method is used to propagate the input uncertainties through the model. The simulation results indicate that the uncertainty propagated to core outlet temperature is about $\pm 10$ °C with a confidence level of 95% in a steady-state operation condition. The result should be noted in the design, operation and code validation of molten salt reactor. In addition, more experimental data is necessary for quantifying the uncertainty of thermophysical properties of molten salts.

## 1. Introduction

Molten salts, as high temperature heat transport medium, are used in many energy transport system. With a volumetric heat capacity about same as that of water, a thermal conductivity and density about twice that of water, and a viscosity roughly three times that of water, fluoride salts have adequate heat transfer characteristics in molten salt reactor [1]. In the Aircraft Nuclear Propulsion (ANP) project at the Oak Ridge National Laboratory (ORNL), the fuel salt, a mixture of the fluorides of sodium, zirconium and uranium ($NaF–ZrF_4–UF_4$), was circulated around a closed loop as a heat transport medium [2]. In the Molten-Salt Reactor Experiment (MSRE), the circulating fuel is a mixture of the fluorides of lithium, beryllium, zirconium, uranium and thorium ($LiF–BeF_2–ZrF_4–ThF_4–UF_4$), the coolant salt is a mixture of the fluorides of lithium and beryllium, the heat generated in reactor core is transferred from the fuel salt to the coolant salt [3]. In the conceptual design study of Molten-Salt Breeder Reactor (MSBR), the fuel salt is $LiF–BeF_2–ThF_4–UF_4$, and the coolant salt selected for the design is $NaBF_4–NaF$ [4]. In order to study the heat transfer characteristics of molten salts, which are generally characterized by low vapor pressures, high melting points and good thermal properties, many experiments are carried out. Grele investigated the forced convection heat transfer characteristics of the eutectic mixture of sodium, potassium and lithium fluoride (FLiNaK, NaF–KF–LiF, 11.5-42.0-46.5 mole percent) flowing through an Inconel X test section [5,6]. Hoffman investigated the heat transfer of molten salts (the mixtures $NaNO_2–NaNO_3–KNO_3$, known as "HTS", FLiNaK and FLiNaK and $NaF–ZrF_4–UF_4$) flowing in forced convection in Inconel tubes [7,8]. Cooke investigated the forced convection heat transfer of mixed fluoride salts ($LiF–BeF_2ThF_4–UF_4$) in a smooth Hastelloy N tube [9]. Ignat studied the heat transfer of FLiNaK in a circular vertical tube [10]. Silverman determined the heat transfer coefficients of two molten-fluoride salts ($LiF–BeF_2–Th_4–UF_4$ and $NaBF_4–NaF$) in a forced convection loop [11]. Yoder determined the heat transfer coefficient of FLiNaK in a small natural circulation cell [12]. Vriesema performed FLiNaK heat transfer in an annular air-to-salt heat exchanger [13]. In the determination of the heat transfer coefficients for molten salts flowing in a liquid-salt heat transfer (LSHT) system, the thermophysical properties of liquid molten salts are essential part of calculation. In different experiments for verifying the heat transfer correlation of liquid salts, different values of the properties of same liquid salt are used to analyze the experimental data, and different heat transfer coefficients are obtained. But some physical properties of the salt are known to be incorrect [14]. Ambrosek reevaluates the data from different convective heat transfer experiments with FLiNaK using different fluid properties, finds that the heat transfer coefficients

---

* Corresponding author.
  *E-mail address:* zouyang@sinap.ac.cn (Y. Zou).

**Table 1**
The physical property data for FLiNaK used by different investigators. $T$: °C, $\rho$: kg/m$^3$, $c_p$: J/(kg · K), $\lambda$: W/(m · K), $\eta$: Pa · s.

| Number | Reference | Property |
|---|---|---|
| 1 | Hoffman, 1995 [19] | $\rho = 2555 - 0.6 \times (T + 273.15)$<br>$c_p = 1890$<br>$\lambda = 4.5$<br>$\eta = 2.5 \times 10^{-5} \times \exp[4790/(T + 273.15)]$ |
| 2 | Grele, 1954 [5] | $\rho = 2555 - 0.6 \times (T + 273.15)$<br>$c_p = 2090$<br>$\lambda = 4.5$<br>$\eta = 2.5 \times 10^{-5} \times \exp[4790/(T + 273.15)]$ |
| 3 | Vriesema, 1979 [13] | $\rho = 2729.4 - 0.73 \times (T + 273.15)$<br>$c_p = 1890$<br>$\lambda = 1.3$<br>$\eta = 1.1 \times 10^{-4} \times \exp[3379/(T + 273.15)]$ |
| 4 | Romatoski, 2017 [18] | $\rho = 2579 - 0.624 \times (T + 273.15)$<br>$c_p = 1884$<br>$\lambda = 0.36 + 0.00056 \times (T + 273.15)$<br>$\eta = 4.0 \times 10^{-5} \times \exp[4170/(T + 273.15)]$ |
| 5 | Yoder, 2014 [20] | $\rho = 2729 - 0.73 \times (T + 273.15)$<br>$c_p = 2010$<br>$\lambda = 0.43 + 0.0005 \times (T + 273.15)$<br>$\eta = 4.0 \times 10^{-5} \times \exp[4170/(T + 273.15)]$ |
| 6 | Ambrosek, 2017 [15] | $\rho = 2729.4 - 0.73 \times (T + 273.15)$<br>$c_p = 1880$<br>$\lambda = 0.36 + 0.00056 \times (T + 273.15)$<br>$\eta = 4.0 \times 10^{-5} \times \exp[4170/(T + 273.15)]$ |
| 7 | Used for TMSR-SF0 | $\rho = 2613.3 - 0.6431 \times (T + 273.15)$<br>$c_p = 1880$<br>$\lambda = 0.36 + 0.00056 \times (T + 273.15)$<br>$\eta = 1.633 \times 10^{-3} \times \exp\left[\dfrac{3.1095 \times 10^{-6} - 2762.9 \times (T + 273.15)}{(T + 273.15)^2}\right]$ |

**Table 2**
The uncertainties for thermophysical property of FLiNaK have a level of confidence of 95% (two standard deviations).

| Property | Uncertainty |
|---|---|
| Density, $\rho$ | 2% |
| Heat capacity, $c_p$ | 10% |
| Thermal conductivity, $\lambda$ | 10% |
| Viscosity, $\eta$ | 10% |

of fluid flowing in the Inconel alloy are in agreement with the Dittus-Boelter correlation when a more accurate thermal conductivity for FLiNaK is used [15]. Several different physical properties data for FLiNaK used in different experiments or analysis are listed in Table 1. Liquid salts density is an important thermal property for assessing the heat transport capability in forced and free convection systems. The density is straightforward to measure and decreases linearly with increasing temperature, now the uncertainty of the measured density of FLiNaK is less than 1% [16]. In the primary loop of molten salt reactor, the temperature drop could be small (between 50 and 100 °C) as a result of the high heat capacity of salts, the empirical method of Dulong and Petit used to predict the heat capacity of salts is accurate to only ±20% [17]. For the fluid transport properties of liquid salts, the viscosity exhibits exponential decrease with reciprocal temperature. The value of thermal conductivity of liquid salt is difficult to measure, which causes error in the analysis of many heat transfer systems. In order to help the design and analysis of nuclear reactor facilities, Romatoski reviews the density, heat capacity, thermal conductivity and viscosity properties for FLiNaK and recommends properties (Number 4 in Table 1) and associated uncertainties (In Table 2), which could be used for modeling to investigate the impacts of property uncertainty on heat transfer system [18].

Uncertainty is an interesting subject, spanning a wide range of scientific domains, such as physics, numerical analysis and computer science [21]. The application of uncertainty analysis in various areas of design and operation of nuclear reactor is increasing, best-estimate computer codes are used to complete the safety analysis of

nuclear reactors [22]. Wang investigates the impacts of uncertainties of thermal-hydraulic parameters on the peak fuel temperature of a small modular molten salt reactor with solid fuel [23]. Zhao analyzes the correlativity about the peak temperature of a liquid-fuel molten salt reactor with thermal-hydraulic parameters by uncertainty analysis method [24]. The uncertainty of thermophysical property of molten salt is a part of the experimental data uncertainties, which can affect the simulation results when a best-estimate calculation with uncertainty quantification is performed [25]. Romatoski uses two test reactor designs (pebble bed and prismatic) to investigate the effects of moltan salts (LiF–BeF$_2$ and NaF–ZrF$_4$) thermophysical property uncertainties on core power [26].

In order to understand the impacts of thermophysical properties uncertainties on the heat transfer characteristics of molten salt reactor facility, guide the design and operation of molten salt reactor, and the validation of computer code. A best-estimate model of a thermal-hydraulic experimental facility is preferred to investigate the effects of thermophysical properties uncertainties of FLiNaK on the thermal-hydraulic parameters.

## 2. The model and methodology

### 2.1. TMSR-SF0 simulator

Molten Salt Reactors (MSR), one of the six Generation-IV designs with intrinsic safety features, operate at high temperatures and near atmospheric pressure [27]. Especially, the fluoride-salt-cooled high-temperature reactors (FHR) attracts more attention as a result of its inherent safety, high economical potential, small modular design, environmental adaptability and nonproliferation [28]. In China, the development of thorium molten salt reactor (TMSR) nuclear energy system has undertaken by the Shanghai Institute of Applied Physics, Chinese Academy of Sciences (SINAP), with the aims of thorium-based nuclear energy utilization and hybrid nuclear energy application [29–31]. Several preliminary designs of solid-fuel and liquid-fuel TMSR were completed, such as a 10 MW Thorium Molten Salt Reactor — Solid Fuel 1 (TMSR-SF1) [32,33]. In 2020, SINAP began the construction of a test reactor with 2 MW nominal thermal power, the Thorium Molten Salt Reactor — Liquid Fuel 1 (TMSR-LF1), in which the nuclear fuel is carried in a mixture of the fluorides of lithium, beryllium and zirconium [34]. TMSR-LF1 will help the construction of large molten salt reactor in the future. In addition, in order to provide essential experimental data for the development of TMSR, a thermal-hydraulic experimental system, the Thorium Molten Salt Reactor — Solid fuel 0 (TMSR-SF0) with a scale of 1:3 of TMSR-SF1, is designed [35,36].

The TMSR-SF0 simulator is an integral effect thermal-hydraulic experimental facility, which consists of two heat transport loops. A simplified overview of the simulator is shown in Fig. 1. In primary loop, the heat source is the reactor core using electric heating rods, the heat sink is the intermediate heat exchanger (IHX), the primary pump circulates the liquid salt (FLiNaK) for transferring heat from the core to IHX. In secondary loop, the heat source is the IHX where two coolant salts exchange heat. The coolant salt is circulated by the secondary pump and flows through the radiator (heat sink), the cooling air is supplied to the radiator by blowers. Finally, the heat generated in core is transferred to air. As a final heat sink, the passive residual heat removal system (PRHRS) surrounds the core vessel, it is used for discharging afterheat in core vessel into atmosphere by means of thermal radiation and free convection. The piping is furnished with insulation (aluminum silicate fiber) to minimize heat loss. The two drain tank provide for the safe storage of the coolant salts when the experiment is suspended. In addition, the loop preheating system (not shown in this figure) using electrical resistance-type heaters, preheats the two liquid-salt loops. The design parameters of SF0 are shown in Table 3. More details about TMSR-SF0 could be found in literature [37–39].
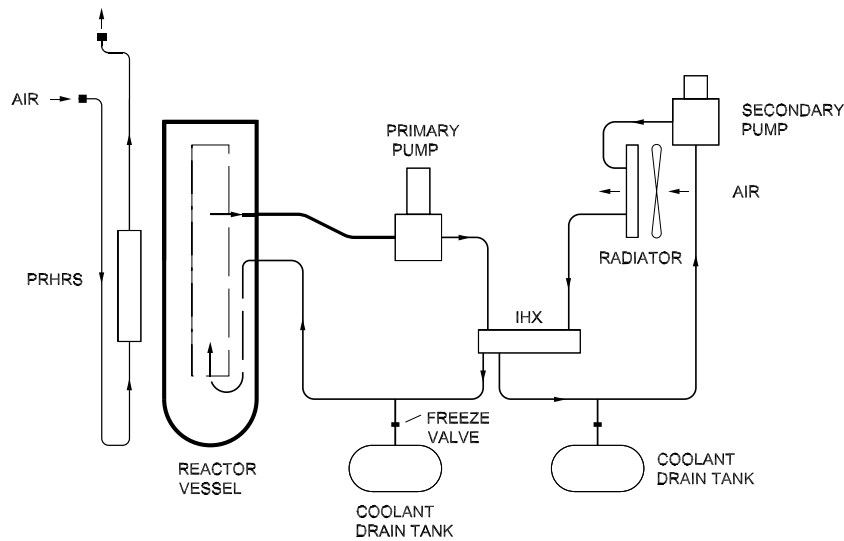
**Fig. 1.** Coolant salts flow diagram of simulator.

**Table 3**
Design operation condition of TMSR-SF0 and simulation result.

| Parameter | Design | Simulation |
|---|---|---|
| Heating power (kW), $P$ | 370 | 370 |
| Core inlet temperature (°C), $T_{1,in}$ | 600.0 | 599.7 |
| Core outlet temperature (°C), $T_{1,out}$ | 650.0 | 650.4 |
| IHX inlet temperature of secondary loop (°C), $T_{2,in}$ | 520.0 | 520.2 |
| IHX outlet temperature of secondary loop (°C), $T_{2,out}$ | 536.0 | 536.4 |
| Radiator air inlet temperature (°C), $T_{air,in}$ | 40.0 | 40.0 |
| Radiator air outlet temperature (°C), $T_{air,out}$ | 180.0 | 180.8 |
| Coolant in primary loop | FLiNaK | FLiNaK |
| Coolant in secondary loop | FLiNaK | FLiNaK |
| Mass flow rate in primary loop (kg/s) $\dot{m}_1$ | 3.9 | 3.897 |
| Mass flow rate in secondary loop (kg/s) $\dot{m}_2$ | 12.2 | 12.198 |
| Pressure drop in primary loop (MPa), $dp_1$ | 0.056 | 0.082 |
| Pressure drop in secondary loop (MPa), $dp_2$ | 0.40 | 0.547 |
| Radiator air mass flow rate (kg/s), $\dot{m}_{air}$ | 2.6 | 2.6 |

**Table 4**
Heat transfer correlations of molten salt and air.

| Fluid | Site | Heat transfer formula | Reynolds number ($Re$) |
|---|---|---|---|
| FLiNaK | Tube side | $Nu = 1.86Re^{0.33}\,Pr^{0.33}$ | $Re < 2300$ |
| | | $Nu = 0.012(Re^{0.87} - 280)\,Pr^{0.4}$ | $2300 < Re < 10^6$ |
| | | $Nu = 0.027Re^{0.8}\,Pr^{0.33}$ | $Re > 10^6$ |
| | Shell side | $Nu = 1.04Re^{0.6}\,Pr^{0.36}$ | $1 < Re < 500$ |
| | | $Nu = 0.71Re^{0.5}\,Pr^{0.36}$ | $500 < Re < 10^3$ |
| | | $Nu = 0.35Re^{0.6}\,Pr^{0.36}$ | $10^3 < Re < 10^5$ |
| Air | Shell side | $Nu = 0.90Re^{0.4}\,Pr^{0.36}$ | $1 < Re < 100$ |
| | | $Nu = 0.52Re^{0.5}\,Pr^{0.36}$ | $100 < Re < 1000$ |
| | | $Nu = 0.27Re^{0.63}\,Pr^{0.36}$ | $1000 < Re < 2.0 \times 10^5$ |

**Table 5**
The simulation results using different thermophysical properties of FLiNaK.

| Parameter | | | | Simulation | | | |
|---|---|---|---|---|---|---|---|
| Number | 1 | 2 | 3 | 4 | 5 | 6 | 7 |
| $P$ (kW) | 370 | 370 | 370 | 370 | 370 | 370 | 370 |
| $T_{1,in}$ (°C) | 555.4 | 555.1 | 587.5 | 605.5 | 601.7 | 603.9 | 599.7 |
| $T_{1,out}$ (°C) | 607.4 | 602.0 | 637.5 | 656.9 | 648.6 | 654.0 | 650.4 |
| $T_{2,in}$ (°C) | 510.8 | 510.9 | 516.6 | 521.5 | 520.6 | 521.0 | 520.2 |
| $T_{2,out}$ (°C) | 526.8 | 525.4 | 532.4 | 537.8 | 535.5 | 536.9 | 536.4 |
| $T_{air,in}$ (°C) | 40.0 | 40.0 | 40.0 | 40.0 | 40.0 | 40.0 | 40.0 |
| $T_{air,out}$ (°C) | 181.1 | 181.1 | 180.9 | 180.8 | 180.8 | 180.8 | 180.8 |
| $\dot{m}_1$ (kg/s) | 3.793 | 3.796 | 3.935 | 3.838 | 3.949 | 3.944 | 3.897 |
| $\dot{m}_2$ (kg/s) | 12.321 | 12.331 | 12.472 | 12.074 | 12.460 | 12.455 | 12.198 |
| $dp_1$ (MPa) | 0.084 | 0.084 | 0.085 | 0.082 | 0.084 | 0.084 | 0.082 |
| $dp_2$ (MPa) | 0.537 | 0.537 | 0.560 | 0.542 | 0.559 | 0.559 | 0.547 |
| $\dot{m}_{air}$ (kg/s) | 2.6 | 2.6 | 2.6 | 2.6 | 2.6 | 2.6 | 2.6 |

### 2.2. Simulation model

The RELAP5 is a best-estimate transient analysis computer code for LWR systems, it can be used for the simulation of thermal-hydraulic transients in both nuclear and nonnuclear systems [40]. The RELAP5-TMSR is an extended version based on RELAP5/MOD4.0. In order to simulation of molten salt reactor systems, thermophysical properties of molten salts (liquid and vapor), new heat transfer correlations, an internal heat source model and a volume ratio neutron kinetics model were implanted in RELAP5-TMSR code [41–44]. And many simulations of transients in TMSR systems were analyzed with the code, such as loss of coolant, anticipated transients without scram (ATWS) and station blackout [45,46]. Thus, the RELAP-TMSR code can be used for simulation of thermal-hydraulic transients of the simulator.

In Fig. 2, a basic RELAP5 nodalization of SF0 model is separated into four sections, PRHRS, primary loop, secondary loop and radiator shell side. The coolant salts in both primary and secondary loops are FLiNaK, the fluids in radiator shell side and PRHRS are air. The physical properties of FLiNaK used for the simulator are shown in Table 1 (Number 7), the heat transfer correlations of molten salt and air are presented in Table 4. Several simplifications have been made for the model, heating rods in reactor core are coalesced into one cylindrical rod, heat exchange tubes in IHX and radiator are coalesced to single tube respectively. Even so, the key thermal-hydraulic parameters are not affected by the simplification, such as the hydraulic diameter of heat exchange tubes, and the flow velocity in loops. In Table 3, the simulation results are closed to the design value of simulator in a same

steady-state condition, it shows that the simulation model could be used for the analysis of the simulator. And the model has been applied for the analysis of steady-state and transient of TMSR-SF0 in previous work [37].

### 2.3. Uncertainty propagation of thermal-properties

The thermophysical properties of FLiNaK in Table 1 (Number 7) are used in the design of the simulator and model. The simulation results shown in Table 3 are close to the design value for the simulator in a same steady-state operation condition. The numerical differences between design and simulation are small, temperature differences are less than 1 °C. In order to understand the impact of thermophysical properties on the heat transfer characteristics of the simulator system, all the properties in Table 1 for FLiNaK are applied to modeling and the
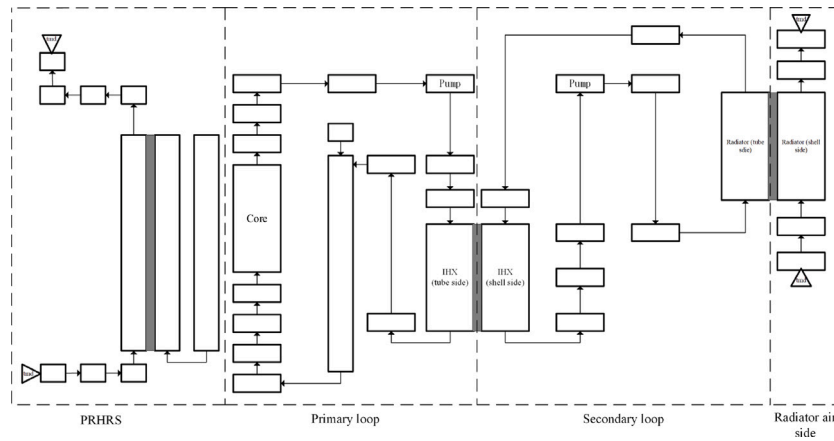
**Fig. 2.** RELAP5 nodalization of TMSR-SF0 system.

results of simulation in the same steady-state operation condition are shown in Table 5. The simulation of Number 1 in Table 5 relates to the properties of Number 1 in Table 1. The heat capacity of Number 1 is different from that of Number 2 in Table 1, which leads to the difference in the temperature difference between inlet and outlet in primary loop or secondary loop. According to the energy balance equation (Eq. (1)), where the heat transfer rate is $\dot{Q}$, $c_p$ is heat capacity, $\dot{m}$ is mass flow rate of fluid and the temperature difference is $T_{out} - T_{in}$. At constant heating power and mass flow, temperature difference is inversely proportional to heat capacity. Thus, the temperature difference in primary loop or secondary loop of Number 1 in Table 5 is great than that of Number 2. On the other hand, different densities for coolant will affect the calculation of mass flow rate in loops when the volume flow rate is constant, the discrepancies could be found on $\dot{m}_1$ and $\dot{m}_2$ in Table 5.

$$\dot{Q} = c_p \dot{m}(T_{out} - T_{in}) \tag{1}$$

In the calculation of heat transfer coefficient of fluid flowing in a tube, some dimensionless number are used. The Nusselt number ($Nu = \alpha L/\lambda$), Reynolds number ($Re = \upsilon L\rho/\eta$) and Prandtl ($Pr = \eta c_p/\lambda$), $\upsilon$ is velocity of fluid, $L$ is the characteristic length and $\alpha$ is the heat transfer coefficient need to be determined. A general correlation for the three number is $Nu = a_1 Re^{a_2} Pr^{a_3}$, and the heat transfer correlations for molten salt and air are listed in Table 4. In general, the heat transfer coefficient has a positive correlation with the thermal conductivity, which means that the temperatures for coolant salt will be low relatively if a high thermal conductivity is used in simulation. A distinct discrepancy could be found between the simulation Number 1 or 2 and the rest in Table 5, and the impact of thermal conductivity has been analyzed by Ambrosek [15]. On the other side, the smaller differences in thermophysical properties used in simulation, the smaller differences in results will be obtained, a example is the comparison of the Number 4, 5, 6, 7 in Table 5. Thus, it is necessary to investigate the uncertainties for a thermal hydraulic analysis of the simulator come from the uncertainties of thermophysical properties. The properties of liquid FLiNaK in Table 1 (Number 4) recommended by Romatoski are used in the simulation model and their uncertainties (in Table 2) with a level of confidence of 95% are incorporated in the inputs to compute its impacts on the heat transfer characteristics of simulator [47].

Eq. (2) is a practicable way that incorporates the uncertainties of thermophysical properties shown in Table 2 into the properties in Table 1 (Number 4). $X_i(T)$ denotes the correlation of the properties with temperature, $i = 1, 2, 3, 4$ relate to density, heat capacity, thermal conductivity and viscosity respectively, $\epsilon_i$ is the uncertainty of property, $X'_i(T)$ can be regarded as a shifted line from $X_i(T)$ when the value of $\epsilon_i$ is determined. The $\epsilon_i$ will be sampled from a normal distribution, $N(\mu, \sigma_i^2)$, the parameter $\mu$ is the mean and the $\sigma_i$ is the standard

deviation. According to the uncertainties provided in Table 2, a 95% confidence level would equal two standard deviations ($2\sigma_i$). For all four input parameters, $\mu = 1$, $\sigma_1 = 0.01$ for that of density, $\sigma_i = 0.05$ ($i = 2, 3, 4$) for that of the rest properties.

$$X'_i(T) = \epsilon_i X_i(T) \quad (i = 1, 2, 3, 4) \tag{2}$$

The thermophysical properties uncertainties can be propagated through the model and a quantifiable uncertainty statistic for interest output parameters is necessary. The uncertainty quantification method used in the work is the Monte Carlo (MC) method, which is the most common forward method and random sampling is used for each uncertainty of thermophysical property $\epsilon_i$ from its normal distribution. The uncertainty of each input will propagate to the output parameters through the model after the simulation is executed many times. The MC method relies on repeated random sampling, which means that the computer code has to be ran numerous times. In order to obtain a desired tolerance limit with confidence for the outputs and reduce computational investment, the Wilks' non-parametric method is applied for determining the sample size and predicting the tolerance limits [48]. The value of the sample size $N$ should be great than 93 for having the probability 0.95 that at least the proportion 95% of the population is included in the two-sided tolerance interval with the upper and lower tolerance limits use the maximum and minimum of the sample [49].

In Fig. 3, the process of uncertainty propagation is shown. Statistical methods are applied to quantify the variability of the results when all input decks are executed by RELAP5 code. In general, the quantification is performed by estimating statistical quantities of outputs, such as mean, maximum and minimum value, and statistical distribution.

## 3. Results and analysis

The effect of uncertainty of thermophysical properties on the simulator system are able to quantify in a steady-state condition. The control parameters (heating power and flows of fluids) are unchanged in time, and the operation condition of the system has to be controlled at a safety level. Thus, an appropriate case is that the heating power is $P = 320$ kW, air mass flow rate is $\dot{m}_{air} = 1.87$ kg/s, the rotational speed of coolant pumps in primary and secondary loops are unchanged, the case is called Case 1. In Case 1, the sample size is $N = 150$, which is over 93 with a two-side tolerance interval (95%/95%). The input samples are plotted in Fig. 4. There are four input parameters, $\epsilon_i (i = 1, 2, 3, 4)$, denoting the uncertainties of thermophysical properties sampled from normal distributions. There are six output parameters, the core inlet temperature $T_{1,in}$, core outlet temperature $T_{1,out}$, IHX inlet temperature of secondary loop $T_{2,in}$, IHX outlet temperature of secondary loop $T_{2,out}$, flow velocity of IHX tube side in primary loop $\upsilon_1$ and velocity of IHX
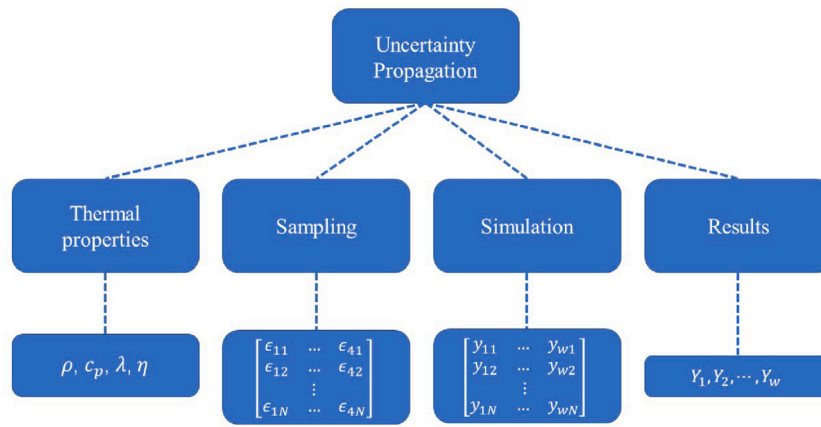
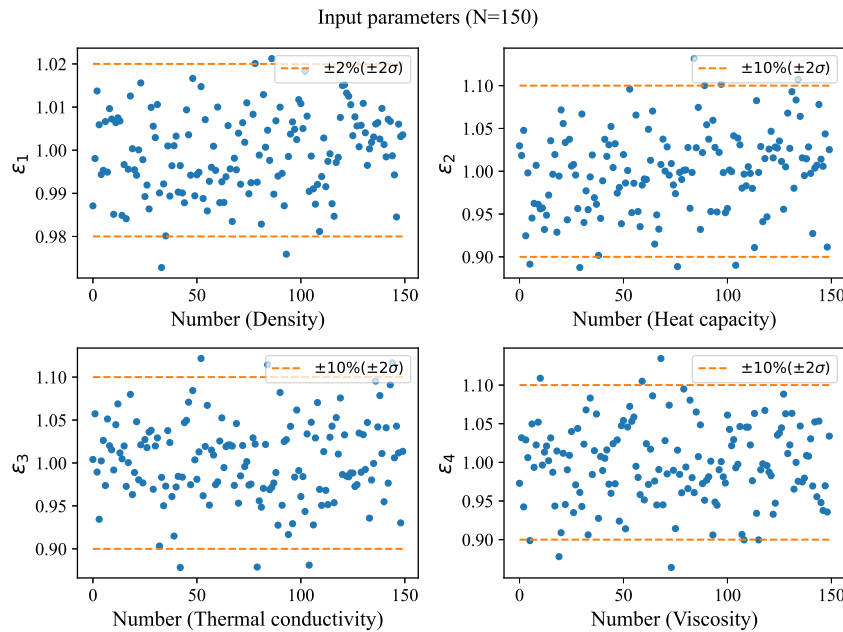**Fig. 3.** The uncertainty propagation process.



**Fig. 4.** Scatter plots of input samples.

shell side in secondary loop $v_2$, could be measured by thermocouples and flowmeters in experiment. The simulation results will be collected and analyzed using several approaches in the work.

In Fig. 5, four histograms show distributions of the temperatures, $T_{1,in}$, $T_{1,out}$, $T_{2,in}$ and $T_{2,out}$. Each histogram has ten bins and every bin in graph is of equal size. The abscissa axis represents temperature. On the vertical axes, it denotes the number of data points fall into each interval. It is clear that all the four histograms are unimodal. Then, some simple statistical analysis are presented in Table 6. For the core outlet temperature $T_{1,out}$, the minimum is 651.1 °C, maximum is 675.0 °C, the variation of core outlet temperature caused by uncertain inputs is 23.9 °C, it means that the uncertainties of inputs lead to a 95% two-side tolerance interval of 651.1 °C and 675.0 °C with confidence level of 95%. The standard deviation for $T_{1,out}$ is 4.6 °C, it is the maximum among the four temperature standard deviations listed in Table 6, which means that the uncertainty of core outlet temperature is the widest .

In simulation and experiment, the unmeasured mass flow rate can be calculated by volume flow rate and density of salt. But the value of mass flow rate is uncertain as a result of the uncertainty of density. The statistic of mass flow rates in primary and secondary loops ($\dot{m}_1$ and $\dot{m}_2$) collected from simulation results shown in Table 6. Mass flows

**Table 6**
Statistics of output variables.

| Parameter | Mean | Minimum | Maximum | Standard deviation |
|---|---|---|---|---|
| $T_{1,out}$, °C | 663.8 | 675.0 | 651.1 | 4.6 |
| $T_{1,in}$, °C | 619.4 | 627.1 | 610.9 | 3.2 |
| $T_{2,in}$, °C | 550.1 | 553.2 | 544.1 | 2.3 |
| $T_{2,out}$, °C | 564.3 | 568.7 | 557.3 | 2.5 |
| $\dot{m}_1$, kg/s | 3.838 | 3.948 | 3.719 | 0.047 |
| $\dot{m}_2$, kg/s | 11.982 | 12.297 | 11.605 | 0.135 |
| $v_1$, m/s | 1.2533 | 1.2594 | 1.2482 | 0.0021 |
| $v_2$, m/s | 0.6892 | 0.6898 | 0.6885 | 0.0002 |

in primary loop ($\dot{m}_1$) are in 3.719-3.948 kg/s range, the uncertainty is $[-3.1\%, +2.9\%]$.

Correlations are used to determine if the relationship between two data sets is causal. Hence, two correlation coefficients, the Spearman's rank correlation coefficient $r_s$ and the Pearson correlation coefficient $r_p$, are applied to measure relationships between inputs and outputs. The Spearman's coefficient is used to assess if the relationship between two variables is monotonic. When the value of $r_s$ is +1 or −1, it means that one of the variables is a perfect monotone function of the other.
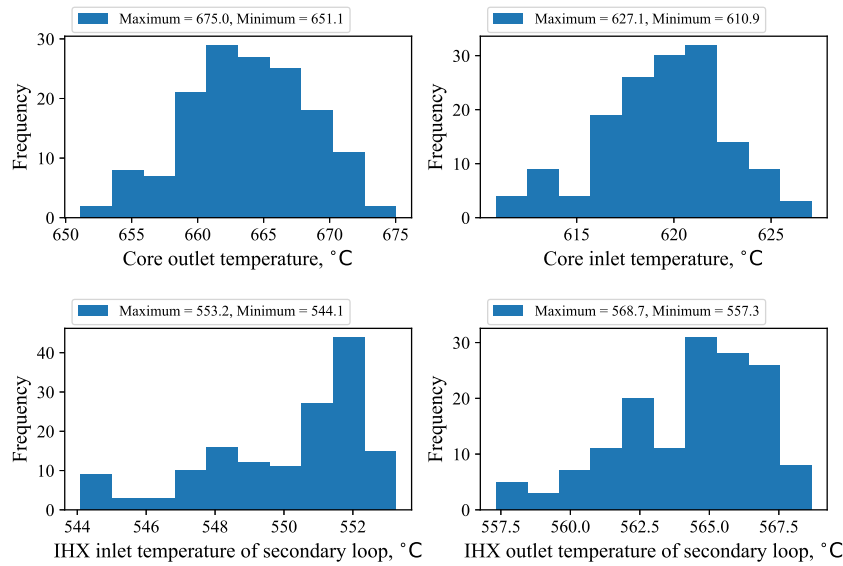
Simulation results (coolant salt temperature)



**Fig. 5.** Frequency distribution of coolant salts temperature.
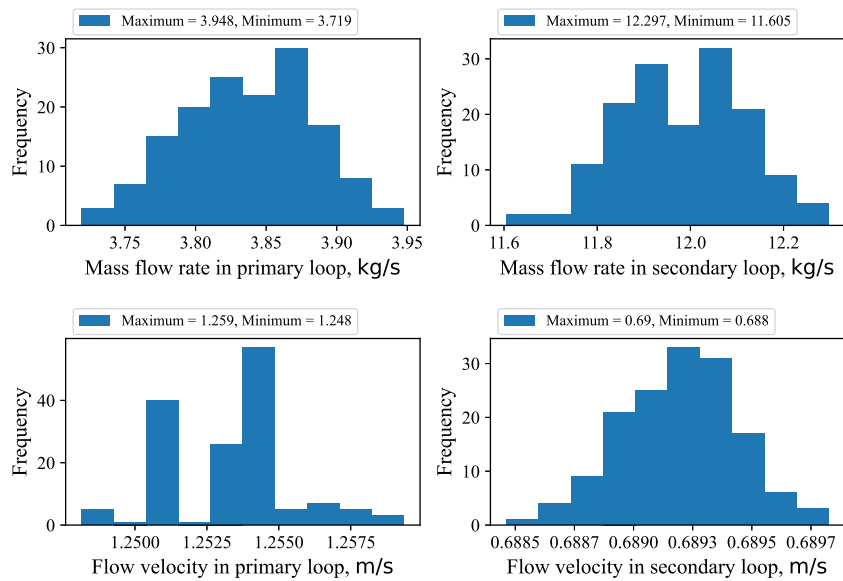
Simulation results (coolant salt flow)



**Fig. 6.** Frequency distribution of mass flow rate and flow rate in primary and secondary loops.

The Spearman's coefficient $r_s$ and Pearson coefficient $r_p$ between $\epsilon_1$ and $\dot{m}_1$ are 0.978 and 0.981 respectively, it is a positive correlations corresponds to an increasing monotonic trend between the uncertainty of density and mass flow rate in primary loop. The $r_s$ and $r_p$ between $\epsilon_1$ and $\dot{m}_2$ are 0.997 and 0.998, it is a same correlation. The correlation coefficients present distinct effects of the uncertainty of density on the mass flow rate. The standard deviations of mass flow in primary and secondary loops are $0.047 \, \mathrm{kg/s}$ and $0.135 \, \mathrm{kg/s}$ respectively. In contrast, The $r_s$ between $\epsilon_1$ and flow velocities ($v_1$ and $v_2$) are small (0.063 and 0.251), both standard deviations of flow velocities ($v_1$ and $v_2$) are so small that simulation results close to the mean. The effect of uncertain inputs on flow velocity is not obvious and the flow rates could be regarded as constant. the histograms of flow velocities and mass flow rates are shown in Fig. 6.

In general, the impact of uncertainties on velocity flow is small, but have an obvious influence on the fluid temperature, especially the core

outlet temperature. Thus, it is necessary to analyze the relationship between the inputs and core outlet temperature. In Fig. 7, it shows the Spearman correlation between input uncertainties and core outlet temperature, the effect of the uncertainty of heat capacity on the core outlet temperature is the most obvious, and the second is the viscosity, but the value of correlation coefficient for density is the lowest.

The effects of uncertain inputs on temperatures are complicated, the uncertainties of temperatures propagated from the uncertainties of thermophysical properties of molten salt need an exact quantification, one of approaches is the linear regression analysis, which can be applied to model the relationship between the temperature response and the four input variables.

Four input variables are independent of each other, and the multiple linear regression can be used to model relationships between input variables and temperatures. A general multiple linear regression model
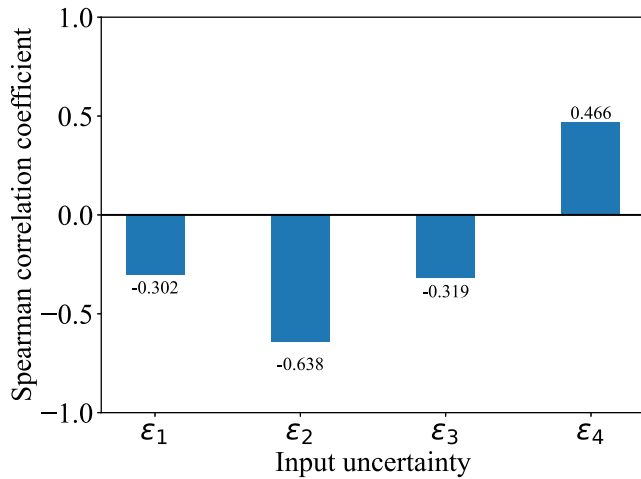
**Fig. 7.** Spearman's rank correlation coefficient between input uncertainties and core outlet temperature.

**Table 7**
Multiple linear regression of core outlet temperature.

| Case | $\beta_0$ | $\beta_1$ | $\beta_2$ | $\beta_3$ | $\beta_4$ | $R^2$ |
|---|---|---|---|---|---|---|
| 1 | 841.3 | −138.6 | −58.6 | −18.5 | 38.2 | 0.735 |
| 2 | 819.8 | −126.2 | −65.0 | −19.3 | 41.3 | 0.946 |
| 3 | 753.6 | −103.7 | −50.7 | −16.9 | 36.6 | 0.997 |

for each data point $j = 1, 2, \ldots, N$ is

$$Y_j = \beta_0 + \beta_1 \epsilon_{1j} + \beta_2 \epsilon_{2j} + \cdots + \beta_i \epsilon_{ij} + \gamma_j \quad (3)$$

The formula (Eq. (3)) consists of uncertain inputs $\epsilon_{ij}$, estimated parameters $\beta_i$, temperature $Y_j$ and the error variable $\gamma_j$, $i = 1, 2, 3, 4$. If the regression model is used to quantify relationship between core outlet temperature $T_{1,out}$ and uncertain inputs, $Y_j$ is the $j$th estimated value of $T_{1,out}$, $\epsilon_{ij}$ is $j$th value of $\epsilon_i$.

Based on the Least-squares estimation, the values of $\beta_i$ ($i = 0, 1, 2, 3, 4$) in regression model for core outlet temperature $T_{1,out}$ are calculated and listed in Table 7. There are three case (1,2,3) simulated in different steady-state operation condition. For Case 1, the heating power is 320.0 kW and the air mass flow is 1.87 kg/s. For Case 2, the heating power and air mass flow are 345.0 kW and 2.32 kg/s respectively. For Case 3, $P = 268.0$ kW and $\dot{m}_{air} = 1.64$ kg/s. The rotational speed of coolant pumps is the same in simulation. According to the regression model of the core outlet temperature $T_{1,out}$ in Case 1, the value of $\sum_{j=0}^{N=4} \beta_j$ denotes the predict result of regression model when all uncertain inputs are not considered in calculation, all of $\epsilon_i$ ($i = 1, 2, 3, 4$) are one, $T_{1,out}$ is 664.7 °C. The results of multiple linear regression analysis show more exactly description of the relationships between uncertain inputs and core outlet temperature than correlation coefficients. The sign of $\beta_i$ ($i = 1, 2, 3, 4$) show the variation tendency of $T_{1,out}$ with the variation of $\epsilon_i$. The numerical value of $\beta_i$ indicate the weight to temperature. For the regression model of $T_{1,out}$, the uncertainty of density ($\epsilon_1$) has most influence on core outlet temperature, all inputs have negative influence except the uncertainty of viscosity.

Regression validation of a regression model is a key step that deciding whether the results of regression model could quantify the relationship between inputs and temperatures. One measure of model validity is the goodness of fit, $R^2$, called coefficient of determination. The general definition of $R^2$ is

$$R^2 = 1 - \frac{SS_{res}}{SS_{tot}} \quad (4)$$

$SS_{res}$ is the sum of squares of residuals, $SS_{res} = \sum_{i=1}^{N}(y_{s,i} - y_{m,i})^2$, $y_{s,i}$ is the $i$th value of simulation results, $y_{m,i}$ is the $i$th fitted value. The total sum of squares, $SS_{tot} = \sum_{i=1}^{N}(y_{s,i} - \bar{y}_s)^2$, $\bar{y}_s$ is the mean of the simulated data. The coefficient of determination $R^2$ normally ranges from 0 to 1, the value of $R^2$ closes to 1 means that the regression model fits the simulation results well. Moreover, for all case of coefficient of determination in Table 7, the value of $R^2$ means that multiple linear regression models are reliable in regression analysis.

## 4. Conclusion

Molten salts have good thermal properties and fluid transport properties, they are used in many energy transport system. In the development of molten salt reactor, the heat transfer of molten salt has been researched for a long time. However, few studies focus on the influence of thermophysical properties uncertainties on the response of molten salt heat transport system. Thus, the uncertainty and sensitivity analysis of the heat transfer characteristics of TMSR-SF0 simulator are carried out on a RELAP5 model.

The thermophysical properties uncertainties of FLiNaK are incorporated in simulation model. The Monte Carlo sampling method is used to propagate the input uncertainties through the model. The uncertainties of density, heat capacity, thermal conductivity and viscosity recommended in literature are ±2%, ±10, ±10% and ±10% respectively. The simulation results indicate that the impact of input uncertainties on volume flow is small, but the effects on temperatures are obvious. There is the probability 95% that at least the proportion 95% of the values of core outlet temperature is included in a two-side tolerance interval of 651.1 °C and 675.0 °C in a steady-state operation condition. It means that the design and operation of molten salt reactor should take note of the variation of core outlet temperature. In the validation of computer code, a part of temperature difference between experimental data and simulation results come from the uncertainties of thermophysical properties of molten salt. In addition, according to the results of multiple linear regression analysis, although the uncertainty of density of FLiNaK has a biggest weight to core outlet temperature, the uncertainty of the heat capacity results in maximum impact as a result of a small uncertainty of density. Hence, more experimental data is necessary for quantifying the uncertainty of thermophysical properties of molten salts.

## Declaration of competing interest

The authors declare that they have no known competing financial interests or personal relationships that could have appeared to influence the work reported in this paper.

## Acknowledgement

## References

[1] D.E. Holcomb, S.M. Cetiner, An overview of liquid-fluoride-salt heat transport systems, ORNL/TM-2010/156, 990239, 2010.
[2] W. Cottrell, H. Hungerford, J. Leslie, J. Meem, Operation of the aircraft reactor experiment, Tech. rep., Oak Ridge National Lab., Tenn., 1955.
[3] R.C. Robertson, MSRE design & operations report part 1 description of reactor design, Tech. rep., Oak Ridge National Lab.(ORNL), Oak Ridge, TN (United States), 1965.
[4] R.C. Robertson, Conceptual design study of a single-fluid molten-salt breeder reactor, Tech. rep., comp.; Oak Ridge National Lab.(ORNL), Oak Ridge, TN (United States), 1971.
[5] M.D. Grele, L. Gedeon, Forced-Convection Heat-Transfer Characteristics of Molten FLiNaK Flowing in an Inconel X System, National Advisory Committee for Aeronautics, 1954.
[6] A. Bergman, E. Dergunov, General phase diagram for KF–LiF–NaF system, Compt. Rend. Acad. Sci 31 (1941) 753–755.

[7] H. Hoffman, J. Lones, Fused salt heat transfer. Part II. Forced convection heat transfer in circular tubes containing NaF-KF-LiF eutectic, Tech. rep., Oak Ridge National Lab.(ORNL), Oak Ridge, TN (United States), 1955.

[8] H. Hoffman, Molten salt heat transfer, Tech. rep., Oak Ridge National Lab., Tenn., 1958.

[9] J. Cooke, B. Cox, Forced-convection heat-transfer measurements with a molten fluoride salt mixture flowing in a smooth tube, Tech. rep., Oak Ridge National Lab.(ORNL), Oak Ridge, TN (United States), 1973.

[10] V. Ignat'Ev, S. Keronovskii, A. Surenkov, O. Shcherbanyuk, S. Manchkha, Y.B. Smirnov, Heat exchange during the flow of a melt of lif- naf- KF fluoride salts in a circular tube, Soviet Atomic Energy 57 (2) (1984) 560–562.

[11] M. Silverman, W. Huntley, H. Robertson, Heat transfer measurements in a forced convection loop with two molten-fluoride salts: LiF–BeF 2–ThF 2–UF 4 and eutectic NaBF 4–NaF, Tech. rep., Oak Ridge National Lab., 1976.

[12] G. Yoder, D. Heatherly, D. Williams, J. Caja, M. Caja, Y. Elkassabgi, J. Jordan, R. Salinas, Liquid fluoride salt experiment using a small natural circulation cell, ORNL/TM-2014/56, Oak Ridge National Laboratory, 2014.

[13] B. Vriesema, Aspects of molten fluorides as heat transfer agents for power generation, 1979.

[14] D. Williams, L. Toth, K. Clarno, C. Forsberg, Assessment of properties of candidate liquid salt coolants for the advanced high temperature reactor (AHTR), ORNL/GEN4/LTR-05-001, 2005, pp. 1–38.

[15] J. Ambrosek, M. Anderson, K. Sridharan, T. Allen, Current status of knowledge of the fluoride salt (FLiNaK) heat transfer, Nucl. Technol. 165 (2) (2009) 166–173.

[16] R.C. Gallagher, C. Agca, N. Russell, J.W. McMurray, N.D. Bull Ezell, Assessment of molten eutectic LiF-NaF-KF density through experimental determination and semiempirical modeling, J. Chem. Eng. Data 67 (6) (2022) 1406–1414.

[17] D.F. Williams, L.M. Toth, K.T. Clarno, et al., Assessment of Candidate Molten Salt Coolants for the Advanced High Temperature Reactor (AHTR), United States. Department of Energy, 2006.

[18] R. Romatoski, L. Hu, Fluoride salt coolant properties for nuclear reactor applications: A review, Ann. Nucl. Energy 109 (2017) 635–647, http://dx.doi.org/10.1016/j.anucene.2017.05.036, URL https://www.sciencedirect.com/science/article/pii/S0306454917301391.

[19] H.W. Hoffman, J. Lones, Fused salt heat transfer Part II: forced convection heat transfer in circular tubes containing NaF-KF-LiF entectic, Tech. rep., ORNL, 1955, ORNL-1777.

[20] G. Yoder, Examination of liquid fluoride salt heat transfer, in: Proceedings of ICAPP, 2014, pp. 6–9.

[21] E. de Rocquigny, N. Devictor, S. Tarantola, Uncertainty in Industrial Practice: A Guide To Quantitative Uncertainty Management, John Wiley & Sons, 2008.

[22] M. Panicker, Licensing and regulatory requirements for best estimate plus uncertainty applications, in: Proc. Int. Conf. Best Estimate Plus Uncertainty (BEPU 2018), 2018, pp. 13–18.

[23] C. Wang, K. Sun, D. Zhang, W. Tian, S. Qiu, G. Su, Thermal-hydraulic design and analysis of a small modular molten salt reactor (MSR) with solid fuel, Int. J. Energy Res. 42 (3) (2018) 1098–1114.

[24] Y. Zhao, Z. Guo, F. Niu, The uncertainty analysis of natural circulation in molten salt reactor coupling dakota with GenFlow, in: International Conference on Nuclear Engineering, Vol. 57847, American Society of Mechanical Engineers, 2017, V006T08A068.

[25] L. Briggs, Uncertainty quantification approaches for advanced reactor analyses, 2009.

[26] R.R. Romatoski, L. Hu, Fluoride-salt-cooled high-temperature test reactor thermal-hydraulic licensing and uncertainty propagation analysis, Nucl. Technol. 205 (11) (2019) 1495–1512.

[27] J. Serp, M. Allibert, O. Beneš, S. Delpech, O. Feynberg, V. Ghetta, D. Heuer, D. Holcomb, V. Ignatiev, J.L. Kloosterman, L. Luzzi, E. Merle-Lucotte, J. Uhlíř, R. Yoshioka, D. Zhimin, The molten salt reactor (MSR) in generation IV: Overview and perspectives, Prog. Nucl. Energy 77 (2014) 308–319, http://dx.doi.org/10.1016/j.pnucene.2014.02.014, URL https://www.sciencedirect.com/science/article/pii/S0149197014000456.

[28] D. Jiang, D. Zhang, X. Li, S. Wang, C. Wang, H. Qin, Y. Guo, W. Tian, G. Su, S. Qiu, Fluoride-salt-cooled high-temperature reactors: Review of historical milestones, research status, challenges, and outlook, Renew. Sustain. Energy Rev. 161 (2022) 112345, http://dx.doi.org/10.1016/j.rser.2022.112345, URL https://www.sciencedirect.com/science/article/pii/S1364032122002581.

[29] M. Jiang, H. Xu, D. Zhimin, Advanced fission energy program-TMSR nuclear energy system, Bulletin of Chinese Academy of Sciences 27 (2012) 366–374.

[30] Z. Dai, Thorium molten salt reactor nuclear energy system (TMSR), in: Molten Salt Reactors and Thorium Energy, Elsevier, 2017, pp. 531–540.

[31] T.J. Dolan (Ed.), Molten Salt Reactors and Thorium Energy, in: Woodhead Publishing Series in Energy, Woodhead Publishing, 2017.

[32] B. Xu, Y. Zou, X. Yu, Y. Fu, Q. Sun, Analysis on ucrw-atws in tmsr-sf1, 2015, URL https://api.semanticscholar.org/CorpusID:195061362.

[33] J. Chen, H. Zhang, Z. Zhu, Coupled neutronic and thermal-hydraulic analysis of TMSR-SF1 at steady state, Nucl. Tech. 40 (2017) 83–90.

[34] Y. Liu, R. Yan, Y. Zou, S. Yu, B. Zhou, X. Kang, J. Hu, X. Cai, Sensitivity/uncertainty comparison and similarity analysis between TMSR-LF1 and MSR models, Prog. Nucl. Energy 122 (2020) 103289, http://dx.doi.org/10.1016/j.pnucene.2020.103289, URL https://www.sciencedirect.com/science/article/pii/S0149197020300482.

[35] H. Xu, Z. Dai, X. Cai, J. Wang, Thorium molten salt reactor and comprehensive utilization of nuclear energy, Mod. Phys. (2018) http://dx.doi.org/10.13405/j.cnki.xdwz.2018.04.007.

[36] G. Zheng, H. Wu, J. Wang, S. Chen, Y. Zhang, Thorium-based molten salt SMR as the nuclear technology pathway from a market-oriented perspective, Ann. Nucl. Energy 116 (2018) 177–186, http://dx.doi.org/10.1016/j.anucene.2018.02.004, URL https://www.sciencedirect.com/science/article/pii/S0306454918300586.

[37] J. Wang, Y. Dai, Y. Zou, H. Xu, Transient analysis of TMSR-SF0 simulator, J. Nucl. Sci. Technol. 58 (3) (2021) 292–301, http://dx.doi.org/10.1080/00223131.2020.1820915.

[38] W. Liu, L. Han, L. Huang, Digital Twin-Driven Development of Online Monitoring and Data Management Systems in TMSR-SF0, in: International Conference on Nuclear Engineering, Volume 12: Innovative and Smart Nuclear Power Plant Design, 2022, http://dx.doi.org/10.1115/ICONE29-92770, V012T12A026.

[39] G. Huang, J. Hou, Y. Liu, W. Lai, B. Li, The development of TMSR-SF0 simulation protection system, in: Y. Xu, Y. Sun, Y. Liu, Y. Wang, P. Gu, Z. Liu (Eds.), Nuclear Power Plants: Innovative Technologies for Instrumentation and Control Systems, Springer Singapore, Singapore, 2020, pp. 112–119.

[40] Information System Laboratories, Inc, Relap5/mod3.3 code manual volumn i: code structure, system models, and solution methods, Tech. rep., 2001.

[41] X. Jiao, K. Wang, Z. He, K. Chen, Core safety discussion under station blackout ATWS accident of solid fuel molten salt reactor, Nucl. Tech. 38 (2015).

[42] S. Jiang, M. Cheng, Z. Dai, G. Liu, Preliminary steady state and transient analysis of a molten-salt based reactor using RELAP/SCDAPSIM/MOD4.0, in: Internal Topical Meeting on Nuclear Reactor Thermal Hydraulics, 2015.

[43] C. Shi, M. Cheng, G. Liu, Development and application of a system analysis code for liquid fueled molten salt reactors based on RELAP5 code, Nucl. Eng. Des. 305 (2016) 378–388, http://dx.doi.org/10.1016/j.nucengdes.2016.05.034, URL https://www.sciencedirect.com/science/article/pii/S0029549316301674.

[44] R. Li, M. Cheng, Z. Dai, Improvement of the delayed neutron precursor transport model in RELAP5 for liquid-fueled molten salt reactor, Nucl. Eng. Des. 394 (2022) 111817, http://dx.doi.org/10.1016/j.nucengdes.2022.111817, URL https://www.sciencedirect.com/science/article/pii/S0029549322001716.

[45] B. Xu, Y. Zou, Q. Sun, X. Yu, Accident analyses of station blackout for TMSR-SF2, Nucl. Tech. 40 (2017).

[46] T. Xu, Y. Zou, B. Xu, G. Zhu, Q. Sun, ATWS accident analysis of rod withdrawal in small modular molten salt reactor, Nucl. Tech. 45 (2022).

[47] R.R. Romatoski, Fluoride-Salt-Cooled High-Temperature Test Reactor Thermal-Hydraulic Licensing and Uncertainty Propagation Analysis (Ph.D. thesis), Massachusetts Institute of Technology, 2017.

[48] S.S. Wilks, Determination of sample sizes for setting tolerance limits, Ann. Math. Stat. 12 (1) (1941) 91–96.

[49] N. Porter, Wilks' formula applied to computational tools: A practical discussion and verification, Ann. Nucl. Energy 133 (2019) 129–137, http://dx.doi.org/10.1016/j.anucene.2019.05.012, URL https://www.sciencedirect.com/science/article/pii/S0306454919302543.